



## Algorithm Development for Full Gaps of Landsat 7 Images

Mohammed I. Abd-ALmajied\*, Loay E. George, Reem Sh. Hameed

Department of Remote Sensing and GIS, College of Science, University of Baghdad. Baghdad, Iraq.

Received: 30/8/2022

Accepted: 27/1/2023

Published: 30/5/2023

### Abstract:

Landsat7 of Enhanced thematic mapper plus (ETM+) was launched on April 15, 1999. Four years later, images start degrading due to the scan line corrector (SLC). SLC is a malfunction that results in pixel gaps in images captured by the sensor of Landsat7. The pixel gap regions extend from about one pixel near the image center and reach up to about 14 pixels in width near the image edge. The shape of this loss is like a zigzag line; however, there are different studies about repairing these gaps. The challenge of all studies depends on retrieving inhomogeneous areas because the homogenous area can be retrieved quickly depending on the surrounding area. This research focuses on filling these gaps by utilizing pixels around them gaps. Pixels from different satellites with the same resolution at the approximate equal date and exact location would be utilized.

Mean and standard deviation were used in gap pixel predicting. For complete pixels gap predicting, an image registration should be applied for predicted a good result—image registration comprised of geometric and radiometric registration. Translation and rotation was the main effect of geometric registration, while pixel tone was mainly related to radiometric registration. Two images of Landsat8 (before and after) with nearly the date of Landsat 7 were used. The fidelity criteria (mean square error and mean absolute error) were utilized to evaluate the results. The results showed a good prediction of the gap pixels in the Landsat 7 image, considering the geometric and radiometric parts.

**Keywords:** Landsat7, Scan Line Corrector, Gap pixel, Image Registration, fidelity criteria.

### طريقة مبتكرة لملئ الفراغات الحاصلة في قمر لاندسات 7

محمد اسماعيل عبد المجيد\*, لؤي ادور جورج, ريم شهاب حميد

قسم التحسس النائي ونظم المعلومات الجغرافية, كلية العلوم, جامعة بغداد, بغداد, العراق

### الخلاصة:

تم اطلاق القمر لاندسات 7 (مصمم الخرائط المواضيعي (ETM+) المحسن في (15/9/1999) وبعد فترة اربع سنوات تم حصول تضرر في الماسح الخطي المصحح (SLC) ان عطل هذا الماسح سبب في حدوث فراغات في بعض البكسلات الخاصه بالصورة الملتقطة بواسطة هذا المتحسس. الفراغات الخاصة بالبكسلات تقريبا تتراوح ما بين البكسل الواحد بالقرب من وسط الصورة الى 14 بكسل بالقرب من الأطراف ويكون شكلها على شكل خط متعرج .

\*Email: [mohammed.ismael@sc.uobaghdad.edu.iq](mailto:mohammed.ismael@sc.uobaghdad.edu.iq)

هناك عدة دراسات تخص ملئ الفراغات الخاصة بالبكسلات بحيث يكون التحدي في عودة الفراغات للمناطق الغير متجانسة على المناطق المتجانسة. ان عودة المناطق المتجانسة تكون نوعا ما اسهل بحيث تعتمد على المناطق المجاورة في تصحيح هذه الفراغات. في هذا البحث تم الاستفادة من البكسلات المجاورة بالإضافة الى صور لنفس المنطقة بنفس الدقة وبتاريخ مقارب ولكن لقمر اخر. تم الاستفادة من المعدل والانحراف المعياري في استعادة الفراغات في البكسلات. لاتمام هذه العملية تم عمل تسجيل لهذه الصور او عمل مطابقة فيما بين صور الأقمار المستخدمة وذلك لكي يتم الحصول على نتائج جيدة. التصحيحات الهندسية والتي تشمل الزحف والتدوير من اهم المشاكل التي تحصل فيما بين صور الاقمار لنفس المنطقة. فيما يكون قيمة البكسل تخص التصحيحات الاشعاعية. صورتين للقمر لاندسات 8 (قبل وبعد تاريخ صورة اللاندسات 7) تم استعمالها. معدل الخطا المربع ومعدل الخطا المطلق تم الاستفادة منهم في حساب معيار الدقة لهذه الطريقة. النتائج أظهرت نتائج جيدة لملئ فراغات البكسلات لصورة القمر لاندسات 7 وبخاصة باخذ بنظر الاعتبار التصحيحات الهندسية والاشعاعية.

## 1. Introduction

Over five decades, the Landsat mission has stayed at the forefront of providing reliable, moderate spatial and temporal resolution imagery of the world. The Landsat program has accomplished the goal and played a crucial part in a wide range of research, including agriculture, forestry, water quality, and geology [1, 2]. As interest in large-scale multi-temporal Landsat data analysis grows, the need to extract as much information as possible from every accessible image [3-5]. It is particularly relevant in the case of the Enhanced Thematic Mapper Plus (ETM+) data from Landsat 7, which launched in April 1999 intending to generate timely and high-quality visible and infrared images of the Earth's surface while it is meeting the mission data continuity goals of previous platforms [6,7]. Unfortunately, the failure of the SLC on board the Landsat 7 enhanced the Thematic Mapper Plus (ETM+) on May 2003. However, it has emerged on the wicked results of data gaps on each Landsat 7 scene permanently, with individual scan lines overlapping each other alternately, causing 22 % of the pixels to be un-scanned and resulting in gaps as large as 14 pixels wide along the scene's edges and gradually decreasing near the scene's center. Correct work would encourage SLC to allow sequent forward and backward scans of ETM + to create a single image.

Nevertheless, neglecting this function can cause recording images in zig-zags sequent along the flight trajectory, resulting in some areas with overlaps and some gaps, as seen in Figure (1) [8, 9]. The bad effects of SLC-off Landsat 7 ETM cause the unusability of images. Several approaches and algorithms for reconstructing the gaps in Landsat 7 SLC-off photos have been proposed to ensure imagery usefulness for multiple applications and the continuity of the Landsat data archive.

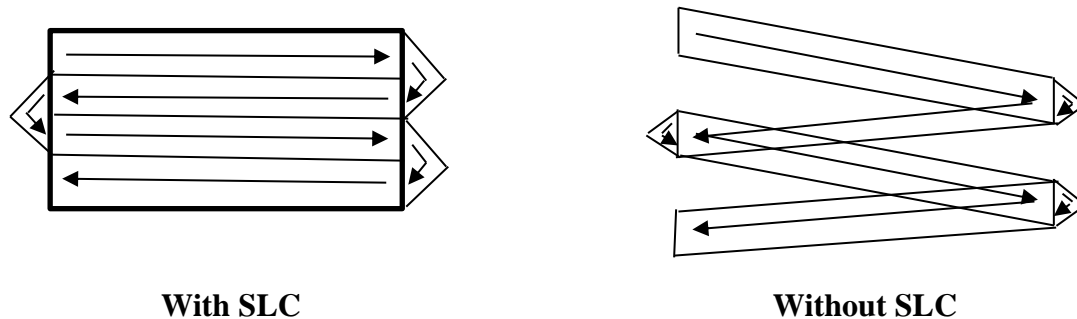


**Figure 1** :Compare with and without SLC.

Ghazali Sulong et al., 2015 used two single-source interpolation approaches, mean and Inverse Distance Weight (IDW) interpolation methods, to estimate the missing pixel value, and the results were compared with a multi-source approach. Also, in Localized Linear Histogram

Match (LLHM), the results were evaluated qualitatively and quantitatively using two statistical markers, root mean square error (RMSE) and systematic error (SE). According to their findings, the LLHM approach outperformed the single-source interpolation method [10]. Gaohong Yin et al., 2016 suggested a gap-filling strategy based on using the Direct Sampling multiple-point geostatistical method. They showed promising results for homogenous regions that may be obtained using non-gap points in the target picture as baseline training data. For diverse landscapes, bivariate simulations using an auxiliary variable obtained separately produce more accurate results than univariate simulations, especially as land cover complexity grows [11]. A work on window regression to mask Operational Land Imager (OLI; Landsat 8) image stacks from five study locations with matching ETM+ missing data layers, which have been used as inputs (Evan B. Brooks et al., 2018).

In addition, a 15×15 pixel window combined with a 9-layer temporal window may yield the most remarkable accuracy. Window regression outperformed the neighborhood-comparable pixel interpolator gap-filling technique in average accuracy [12]. Landsat-7 data was rectified using a focused analysis approach involving the median filtering procedure and a method based on a specific algorithm for applying the filter to pictures. A median filter of 3×3 was used to repair and fix the Landsat 7 picture, and ERDAS imaging software was used to recover the damaged pixels [13]. Salema S. Salman et al., 2020 establish a spatial congruence between pictures by applying image correlation criteria. Over 48 days, three different time pictures and two algorithms were utilized to fill in the gaps. Three photographs were used at separate periods, and for not more than 48 days in the first algorithm, they produced free of gaps images, but in the second method, they obtained free of gaps images for not more than 16 days [14]. This study has established a new algorithm to refill a pixel's gap. It depends on geometric and radiometric parts. All image registration and pixel location can be regarded as a geometric section; the radiometric concern is the contrast distribution.

## 2. Data and Methods

### 2.1. Data and Software

Landsat-7 and Landsat-8 satellite imagery were utilized, particularly regarding the direction covered, obtained from the USGS Earth Explorer database. Table (1), Table (2), and Table (3) show bands of Landsat7 and Landsat8, respectively. Matlab programming language was used in this research.

**Table 1:** The Satellite images of the study area

	Landsat-7 satellite images		Landsat-8 satellite images	
Acquired Date	7/9/2020	30/8/2020	1/10/2020	
Longitude	45° 02' 35."	45° 02' 35"	45° 02' 35"	
Latitude	33° 10' 55"	33° 10' 55"	33° 10' 55"	
Resolution	30 meters	30 meters	30 meters	
Format	GEOTIFF	GEOTIFF	GEOTIFF	
Altitude	705 Km	705 Km	705 Km	
Repeat Cycle	16-day	16-day	16-day	

**Table 2:** Bands of Landsat7 [15].

Landsat 7 ETM +		
Band	Wavelength ( $\mu\text{m}$ )	Resolution (m)
1	0.450 – 0.515	30
2	0.525 – 0.605	30
3	0.630 – 0.690	30
4	0.750 – 0.900	30
5	1.55 – 1.75	30
6	10.40 – 12.50	60
7	2.09 – 2.35	30
8	0.520 – 0.900	15

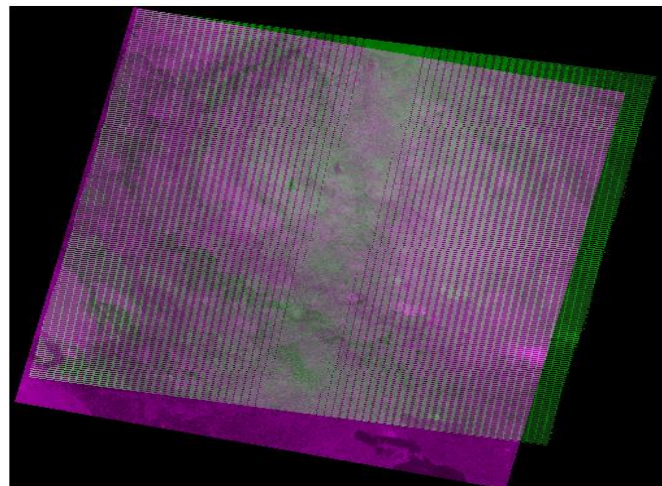
**Table 3:** Bands of Landsat8 oli [16].

Landsat 8 Sensors	Band	Wavelength ( $\mu\text{m}$ )	Resolution (m)
Operational Land Imager (OLI)	1	0.433-0.453	30
	2	0.450-0.515	
	3	0.525-0.600	
	4	0.630-0.680	
	5	0.845-0.885	
	6	1.560-1.660	
	7	2.100-2.300	
	8	0.500-0.680	15
	9	1.360 -1.390	30
Thermal Infrared Sensor (TIRS)	10	10.30 – 11.30	100*
	11	11.50-12.50	
BQA Quality Assessment		BQA Quality Assessment	

\* TIRS bands are acquired at the 100-meter resolution but are resampled to 30 m in the delivered data product.

## 2.2. Methods

Images taken from different versions of Landsat (Landsat7 and Landsat8) need to be registered with each other. The parameters that affect registration are translation and rotation operators. The unregistrable effects can be seen in Figure (2).

**Figure 2:** The two images of Landsat7 and Landsat 8.

The three images have the same resolution (30\*30 m for each pixel). The progress of the algorithm is mentioned below in Figure (3) as follows:

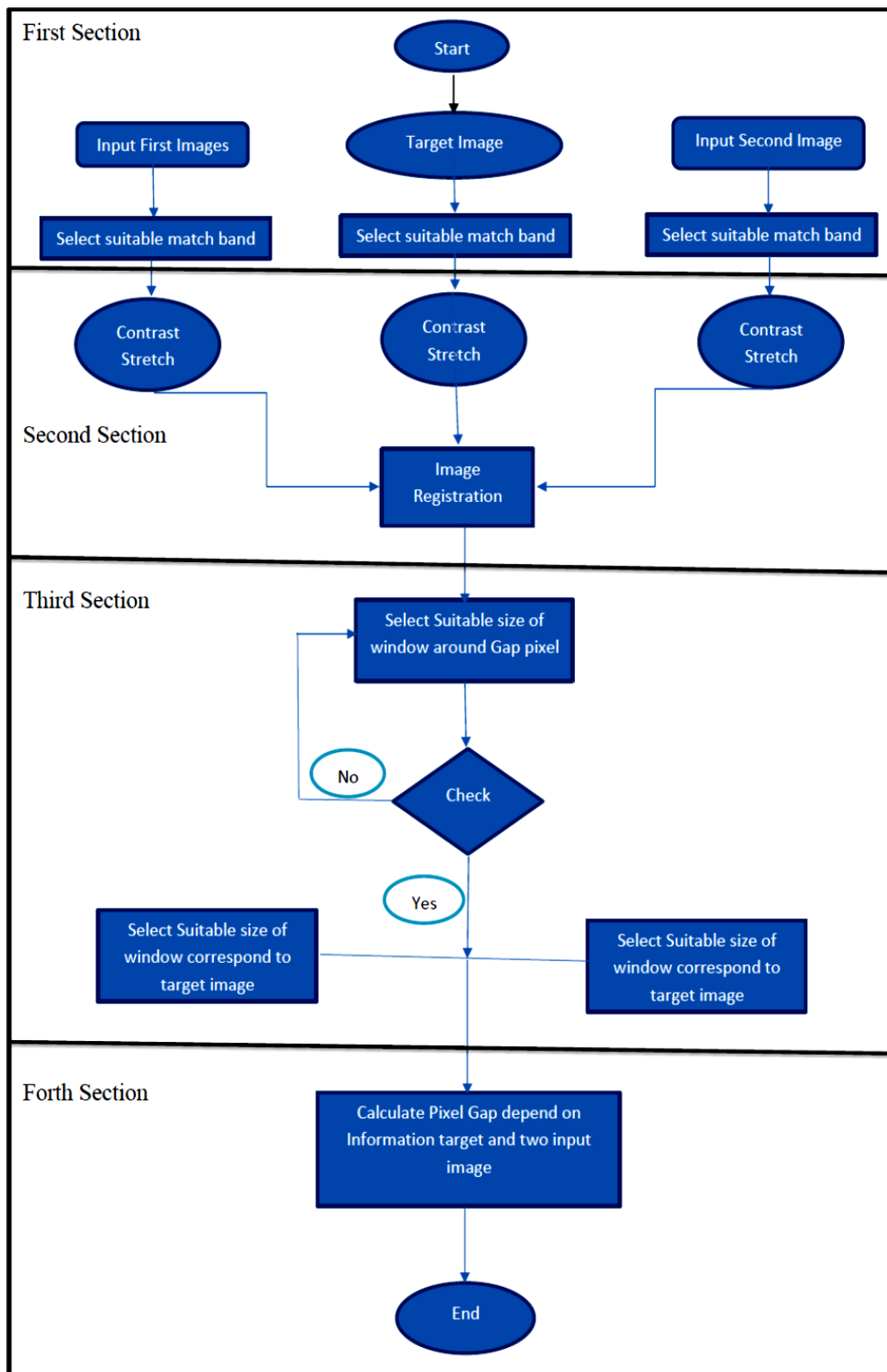


Figure 3: Flow chart of the algorithm

The arrangement of the algorithm is as follows:

### 2.2.1. First section:

The image of Landsat7 was chosen based on a specific year date, which is free from clouds. The other images of Landsat8 were selected at a time close to the target; the band sequence of both satellites was not parallel; Band 1 in Landsat 7 equals band 2 in Landsat 8.

### 2.2.2. Second Section:

The two satellite images were georeferenced with each other, but their images were not precisely matched. The unmatched images refer to small attitude and path differences between satellites. Before calculating the exact location of the pixel gaps, images must be aligned. Also, the scenes' sizes must coincide before being matched.

An algorithm was built to determine the accurate registration between satellite images. Translation and rotation were the most parameters that affected it. In the first part, the translation was determined depending on the absolute mean between the two images. To reduce computation time, an auto-size window was defined. Means were criteria for finding the optimal shifting between two images as shown in the following equation: (mean square error) [17, 18].

$$K = \frac{1}{mn} \sum_{i=1}^m \sum_{j=1}^n |L7_{(i,j)} - L8_{(i,j)}| \quad (1)$$

Where  $(L7_{(i,j)}$  and  $L8_{(i,j)})$  are the selective window of two images.

The second part evaluated a rotation depending on features between two images. In the beginning, The scale-invariant feature transform (SIFT) algorithm was used for detecting points for both images. Different features may be affecting the number and quality of that points. A feature representing maximum intensity showed more stability for calculating image rotation.

$$P_{\max(i,j)} = L_{\max} > L_{(i,j)} > L_{\text{threshold}} \quad (2)$$

Where  $(P_{\max})$  represents the maximum point inside features in both images.

After the image registration, the size of the two images was not equal, which conflicted with the computation. A pixel neighbor was computed; zero-pixel was compared with the corresponding one in the second image with its neighbor. A pixel value would be removed if it did not correspond to other images. The technique was like a seed-filling one and would be applied only on the four edges of both images. As in Figure (4) [19-21], four neighbors were checked.

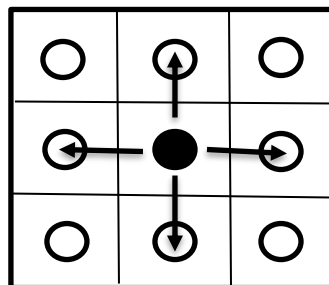


**Figure 4:** Seed Filling.

### 2.2.3. Third Section

The grey values range of both images was elongated by applying the (standardization transform or Z-score) equation before starting the repair; the equation of (Z-score) is [19-22]:

$$\bar{x} = \frac{x - \mu}{\sigma} \quad (3)$$

Where ( $\mu$ ) represents the mean, and ( $\sigma$ ) is the standard deviation.

The window size around the gap pixel is essential for calculating this pixel. The criteria for picking a suitable window size was based on the neighbors of the gap pixel. Selecting a minimum number of points in four quadrants around the gap pixel was its primary condition. Selecting a four-quadrant neighbor assists the brightness and contrast of the gap with its neighbor and makes it more balance with them. Two-point was the minimum condition for each quadrant.

#### 2.2.4. Fourth Section

An algorithm that is used for repairing lost pixels in Landsat7 with the aid of Landsat8 is:

$$\frac{X_1 - \mu_1}{\sigma_1} = \frac{X_2 - \mu_2}{\sigma_2} \quad (4)$$

where  $X_1$ ,  $\mu_1$  and  $\sigma_1$  are the first points in the first image, which are mean points and standard deviation, respectively, for the first image.  $X_2$ ,  $\mu_2$  and  $\sigma_2$  represent the value of the second point, the mean, and the standard deviation for the second image. The mean and standard deviation are determined on a window of different sizes around a selected center point. An evaluated algorithm was used to assess the result.

Mean Squared Error is the mean of the squared prediction errors over all instances in the test set.

The mean squared error (MSE) is calculated from the following equation [23]:

$$MSE = \frac{1}{n} \sum_{i=1}^n (y_i - x_i)^2 \quad (5)$$

Where  $n$  is the number of samples,  $y_i$  is the predicted value,  $x_i$  is the original value of the testing data.

Mean Absolute Error is the mean of the absolute values of the individual prediction errors over all instances in the test set. The mean absolute error (MAE) is calculated from equation (1).

### 3. Results and Discussion

Contrast stretching made the range of gray level the same on both satellite images using equation (3). Image registration was carried out for corresponding images. After that, a crop edge of each image was applied, which can be seen in Figure (5).

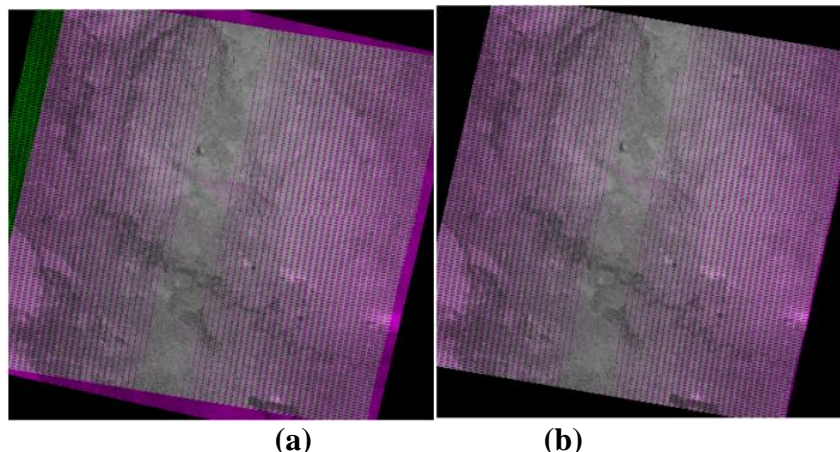


**Figure 5:** a. two registered images, and b. cropping edges of each image.

Landsat7 Gaps were determined with the assistance of two images of Landsat8 using neighbors of pixel gap and then replaced by equation (2). A window of different sizes was used, where the window size depends mainly on the position of the gap pixel. The size of this window used to determine the mean and standard deviation starts from  $(7 \times 7)$  to  $(51 \times 51)$  pixels. This window would be divided into four quarters to determine an equal number of points for the mean and standard deviation computations. The suitable size of the window is picked when there are at least four points in each quarter of the selected window. The final repair of an image of Landsat7 is shown in Figure (6).

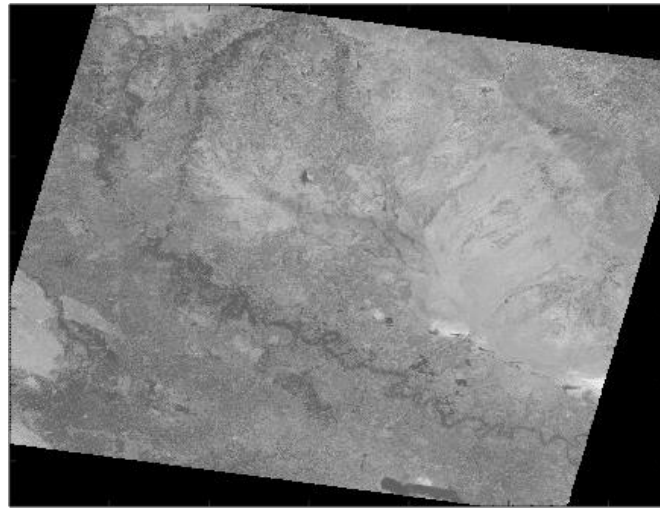


**Figure 6:** Final repaired Landsat7 image

A sample of Landsat7 and Landsat8 were displayed. A part of Landsat7 is present before applying the repairing process. The same parts after the repair process are shown, and the exact position of these parts for Landsat8 is shown just for comparison, Figure (7).

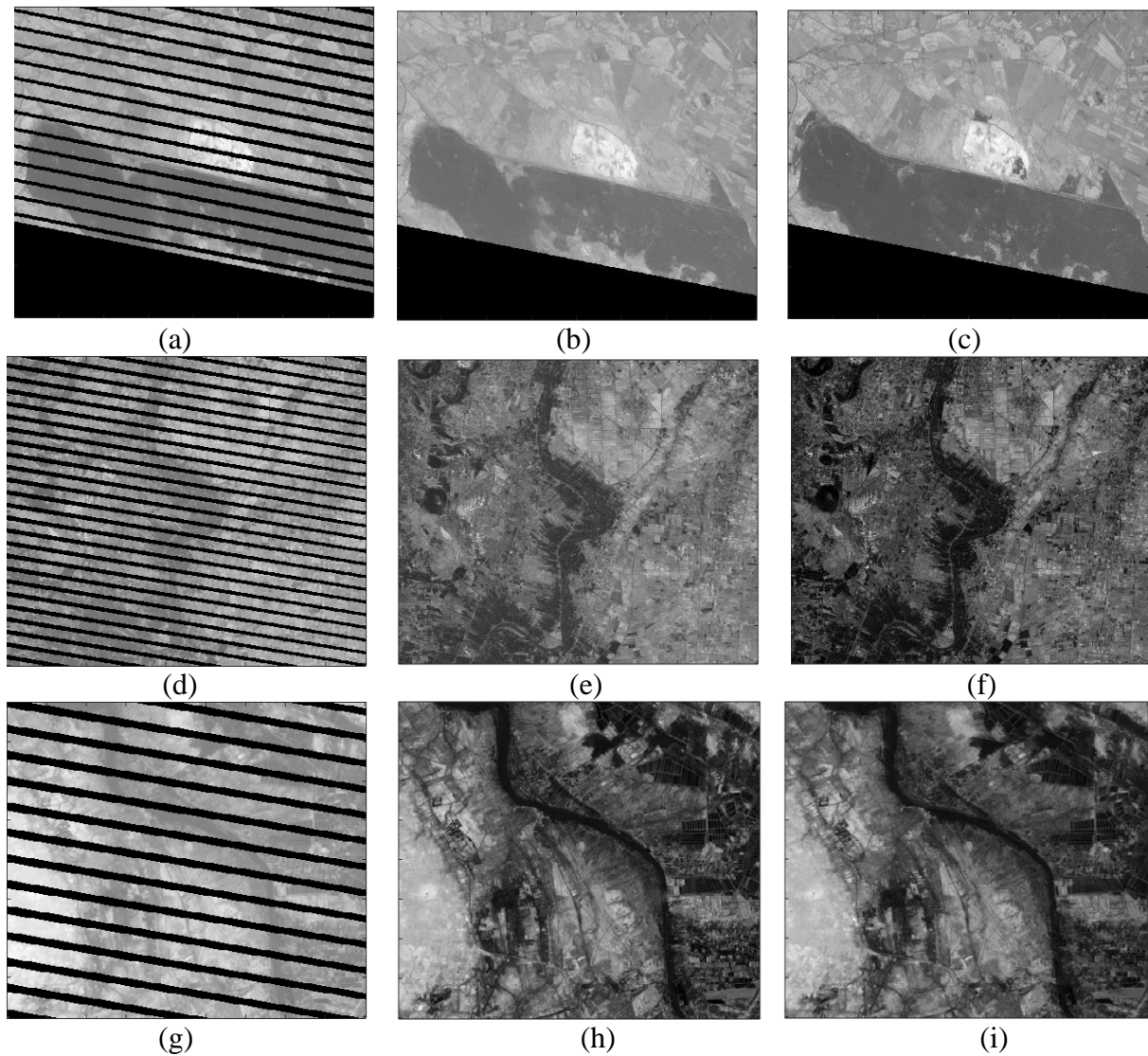


**Figure 7:** (a, d, and g) parts of Landsat7 images before the repairing process, (b, e, and h) parts of Landsat7 images after the repairing process. (c, f, and i) parts of Landsat8 images to compare the repairing one.

Table (4) shows the algorithm's evaluation for non-gap points in the Landsat7 image. The non-gap pixels in Landsat7 were used to check the quality of the process. The results would be compared with the original values. Mean square error and absolute error (equation (5) and equation (1)) were used in the measurement. The determinate measurement is the state between the non-gap pixel and the result using equation (4). The size of windows that were used in this test is  $(11 \times 11)$  and  $(21 \times 21)$ . Table (4) shows the results for a window size of  $(11 \times 11)$  using two images of Landsat8 (before and after) for predicting values. At the same time, Tables (5 and 6) showed results for the same window but for Landsat 8 images before and after, respectively. Table (7) used the window size of  $(21 \times 21)$  for two Landsat8 images (before and after). The results for the same window of Landsat 8 images, before and after, are shown in the Tables (8 and 9).

**Table 4:** Result of mean square error and absolute square error using the window size of (11×11) for Landsat8 image (before and after)

Points No.	Mean square error	Absolute mean square error
100000	42.0332	4.5053
200000	43.3512	4.5942
300000	42.6756	4.5551
500000	42.0478	4.5171
700000	42.4608	4.5378
1000000	42.3836	4.5468

**Table 5:** Result of mean square error and absolute square error using a window size of (11×11) for Landsat8 image (before)

Points No.	Mean square error	Absolute mean square error
100000	45.9546	4.6242
200000	46.5979	4.6919
300000	44.9800	4.6190
500000	43.7113	4.5475
700000	43.8884	4.5516
1000000	43.3679	4.5365

**Table 6:** Result of mean square error and absolute square error using a window size of (11×11) for Landsat8 image (after)

Points No.	Mean square error	Absolute mean square error
100000	67.4210	5.5832
200000	70.9630	5.7425
300000	71.5463	5.7453
500000	72.1645	5.7473
700000	73.0687	5.7935
1000000	73.5694	5.8381

**Table 7:** Result of mean square error and absolute square error using a window size of (21×21) for Landsat8 image (before and after)

Points No.	Mean square error	Absolute mean square error
100000	42.6432	4.5377
200000	43.6265	4.6048
300000	42.8141	4.5629
500000	42.1109	4.5208
700000	42.4949	4.5398
1000000	42.4375	4.5490

**Table 8:** Result of mean square error and absolute square error using a window size of (21×21) for Landsat8 image (before)

Points No.	Mean square error	Absolute mean square error
100000	46.3914	4.6484
200000	46.7471	4.6991
300000	45.0381	4.6221
500000	43.7445	4.5495
700000	43.8983	4.5524
1000000	43.3922	4.5378

**Table 9:** Result of mean square error and absolute square error using a window size of (21×21) for Landsat8 image (after)

Points No.	Mean square error	Absolute mean square error
100000	68.5381	5.6236
200000	71.7460	5.7644
300000	72.0454	5.7619
500000	72.3243	5.7542
700000	73.1471	5.7969
1000000	73.6996	5.8425

The following figures (8 and 9) showed the result in a scatter plot, comparing the predicted and original non-gap points. The scatter plot represents the relationships between predicted points and the original one; the closer to the diagonal, the more related to the real one when data away from the diagonal means no relation persists. Figure (8) represents the result for window size (5×5) for two Landsat images (before and after) with ( $R^2 = 0.9514$ ) and with linear equation ( $y = 1.0167x - 2.1809$ ). Figure (9) for the same images but for a window size of (10×10) with ( $R^2 = 0.9514$ ), with the same equation.

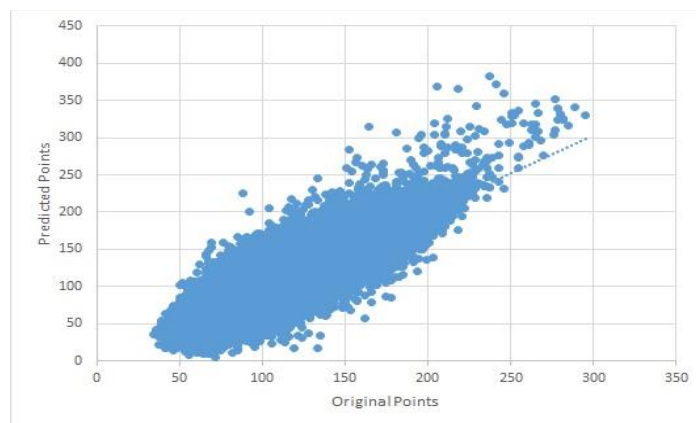


**Figure 8:** Scatter plot between predicted and original points of Landsat 7

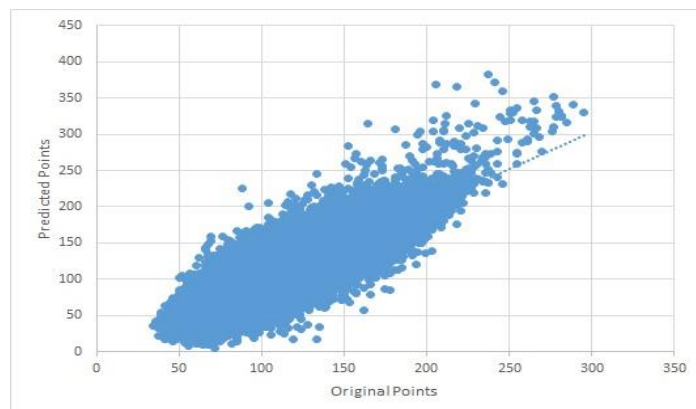


**Figure 9:** Scatter plot between predicted and original points of Landsat 7 using window (21×21) pixels.

#### 4. Conclusion

Landsat7 gaps due to Line scan problems are not constant in their number and position; they have a zigzag shape. The un-constant numbers of gap-pixel made them un-constant in selecting a fixed process for the computation of the lost pixel. The new algorithms for predicting a lost pixel depend on the position of the pixel and the type of signature. An image registration (geometric and radiometric process) must be applied to predict these pixels. First, a geometric correction is applied to extract the exact location of a pixel, including selecting a suitable pixel for the gap location. Using mean and standard deviation is more related to radiometric correction to pick a nice tone of the lost pixel. The final process was the predicted value for the gap pixel. There was always a limitation to the goodness of the process. First, the difference in acquisition time may influence the result and the angle of illumination or sunlight. The degree of purity of the atmosphere also affects obtaining a better result. The reason for selecting two images of Landsat8 is to select an appropriate point better to predict values for lost points. The applied algorithm in this research reveals a promising approach for assessing the values of lost pixels, as seen in the previous figures. The fidelity of this algorithm was shown through the tables of mean square error, and absolute square error, also with the scatter plot, which shows promising approaches.

#### Acknowledgments

I want to acknowledge and thank Dr. Loay E. George, who made this work possible. His idea, guidance, and advice carried me through all the writing stages, and thank you for your thoughtful comments and suggestions. Also, I would like to thank the lecturer Reem Sh. Hameed for her assessment. Finally, I would like to thank God for letting me through all the difficulties.

#### Conflict of Interest

There is no interest conflict.

#### Reference

- [1] M. Wulder and T. Loveland, "Roy, DP Crawford, CJ Masek, JG Woodcock, CE Allen, RG Anderson, MC Belward, AS Cohen, WB Dwyer, J. Erb, A. Gao, F. et al. Current status of Landsat program, science, and applications," *Remote Sensing of Environment*, vol. 225, pp. 127-147, 2019.
- [2] V. Martos, A. Ahmad, P. Cartujo, and J. Ordoñez, "Ensuring agricultural sustainability through remote sensing in the era of agriculture 5.0," *Applied Sciences*, vol. 11, no. 13, p. 5911, 2021.
- [3] S. Wei, H. Zhang, C. Wang, Y. Wang, and L. Xu, "Multi-temporal SAR data large-scale crop mapping based on U-Net model," *Remote Sensing*, vol. 11, no. 1, p. 68, 2019.
- [4] V. Sitokoustantinou, A. Koukos, T. Drivas, C. Kontoes, I. Papoutsis, and V. Karathanassi, "A Scalable Machine Learning Pipeline for Paddy Rice Classification Using Multi-Temporal Sentinel Data," *Remote Sensing*, vol. 13, no. 9, p. 1769, 2021.
- [5] Y. Fang, L. Xu, A. Wong, and D. A. Clausi, "Multi-Temporal Landsat-8 Images for Retrieval and Broad Scale Mapping of Soil Copper Concentration Using Empirical Models," *Remote Sensing*, vol. 14, no. 10, p. 2311, 2022.
- [6] M. Boschetti, F. Nutini, G. Manfron, P. A. Brivio, and A. Nelson, "Comparative analysis of normalised difference spectral indices derived from MODIS for detecting surface water in flooded rice cropping systems," *PloS one*, vol. 9, no. 2, p. e88741, 2014.
- [7] T. Mugiraneza, A. Nascetti, and Y. Ban, "Continuous monitoring of urban land cover change trajectories with landsat time series and landtrendr-google earth engine cloud computing," *Remote Sensing*, vol. 12, no. 18, p. 2883, 2020.
- [8] [8] K. G. Nikolakopoulos and I. Raptis, "Open quarry monitoring using gap-filled LANDSAT 7 ETM SLC-OFF imagery," in *Earth resources and environmental remote sensing/GIS applications V*, 2014, vol. 9245, pp. 32-42: SPIE.

- [9] Y. M. Asare, E. K. Forkuo, G. Forkuor, and M. Thiel, "Evaluation of gap-filling methods for Landsat 7 ETM+ SLC-off image for LULC classification in a heterogeneous landscape of West Africa," *International Journal of Remote Sensing*, vol. 41, no. 7, pp. 2544-2564, 2020.
- [10] G. Sulong and A. Sadiq, "Single and multi-source methods for reconstruction the gaps in Landsat 7 ETM+ SLC-off images," *Research Journal of Applied Sciences, Engineering and Technology*, vol. 11, no. 4, pp. 423-428, 2015.
- [11] G. Yin, G. Mariethoz, and M. F. McCabe, "Gap-filling of landsat 7 imagery using the direct sampling method," *Remote Sensing*, vol. 9, no. 1, p. 12, 2016.
- [12] E. B. Brooks, R. H. Wynne, and V. A. Thomas, "Using window regression to gap-fill Landsat ETM+ post SLC-Off data," *Remote Sensing*, vol. 10, no. 10, p. 1502, 2018.
- [13] W. A. Faeq and A. S. Mahdi, "The Landsat 7 imagery gap filling using median filter method," *Iraqi Journal of Physics*, vol. 17, no. 42, pp. 158-162, 2019.
- [14] S. S. Salman, A. H. Al-Saleh, H. K. Abbas, and A. A. Al-Zuky, "Adaptive method for landsat ETM+ gap filling using successive temporal images," *NeuroQuantology*, vol. 18, no. 2, pp. 112-122, 2020.
- [15] L. P. Flynn, A. J. Harris, and R. Wright, "Improved identification of volcanic features using Landsat 7 ETM+," *Remote Sensing of Environment*, vol. 78, no. 1-2, pp. 180-193, 2001.
- [16] T. D. Acharya and I. Yang, "Exploring landsat 8," *International Journal of IT, Engineering and Applied Sciences Research (IJIEASR)*, vol. 4, no. 4, pp. 4-10, 2015.
- [17] H. Fadaei, R. Suzuki, T. Sakaic, and K. Toriid, "A proposed new vegetation index, the total ratio vegetation index (TRVI), for arid and semi-arid regions," *International Archives of the Photogrammetry, Remote Sensing and Spatial Information Sciences*, vol. 39, p. B8, 2012.
- [18] [18] J. Xue et al., "Mapping daily evapotranspiration at field scale using the harmonized Landsat and Sentinel-2 dataset, with sharpened VIIRS as a Sentinel-2 thermal proxy," *Remote Sensing*, vol. 13, no. 17, p. 3420, 2021.
- [19] [19] A. K. Kuzucu and F. B. Balcik, "Testing the potential of vegetation indices for land use/cover classification using high resolution data," *ISPRS Annals of the Photogrammetry, Remote Sensing and Spatial Information Sciences*, vol. 4, p. 279, 2017.
- [20] [20] R. Alcalde, C. Alonso de Armiño, and S. García, "Analysis of the economic sustainability of the supply chain sector by applying the altman Z-score predictor," *Sustainability*, vol. 14, no. 2, p. 851, 2022.
- [21] [21] M. I. ABD-ALMAJIED, L. E. GEORGE, and K. M. ABOOD, "A PROPOSED METHOD OF SELECTING PAIRS OF SIFT POINTS," *Journal of Theoretical and Applied Information Technology*, vol. 97, no. 3, 2019.
- [22] [22] M. I. Abd-ALmajied, L. E. George, and K. M. Abood, "Rotation Estimation Between Two Images Using Feature Analysis," *IJCSNS*, vol. 19, no. 1, p. 22, 2019.
- [23] [23] H. Wu, M. J. Hayes, A. Weiss, and Q. Hu, "An evaluation of the Standardized Precipitation Index, the China-Z Index and the statistical Z-Score," *International Journal of Climatology: A Journal of the Royal Meteorological Society*, vol. 21, no. 6, pp. 745-758, 2001.